Piezoelectric-Based Power Conversion: Recent Progress, Opportunities, and Challenges

Jessica D. Boles, Joshua J. Piel, Elaine Ng, Joseph E. Bonavia, Jeffrey H. Lang, and David J. Perreault

Massachusetts Institute of Technology

I. Introduction

Pursuits of miniaturization, greater performance, and lower cost for power electronics necessitate advancement of power passive component technologies. While wide-bandgap semiconductor devices and advanced control techniques have enabled substantial size and performance improvements, miniaturizing power electronics remains bottlenecked by the passive components dominating their sizes, particularly magnetics (i.e., inductors and transformers). Magnetic components pose fundamental power handling and efficiency challenges at small scales, amounting to lower power densities at low volume [1-3]. On the other hand, switched capacitor converters have achieved record-breaking power densities and efficiencies, but these architectures still require magnetics for efficient voltage regulation. While several miniaturization strategies have been developed despite the limitations of magnetics (e.g., higher switching frequencies, more sophisticated circuit topologies and operating techniques, and improved magnetic designs), they ultimately still face the same scaling impediments. This motivates investigation into alternative passive component technologies for power conversion that can provide the same high-level functionalities as magnetics but with superior scalability to small sizes.

Piezoelectric components have emerged as alternative power passives that can offer favorable scalability for miniaturization [4-5]. Piezoelectrics store energy in the mechanical compliance and inertia of a piezoelectric material with energy densities several orders of magnitude greater than those of magnetics at small scales. An optimistic theoretical investigation in [4] suggests that piezoelectric components may be capable of handling up to kilowatt-level power within only 1 mm^3, which is unprecedented in power conversion. Piezoelectrics also offer other potential advantages to power conversion including planar form factors, galvanic isolation (with multi-port devices), batch fabrication, and amenability to integration.

Piezoelectric components can be realized as single-port piezoelectric resonators (PRs) or multi-port piezoelectric transformers (PTs). In the proximity of a resonant mode, PRs can be modeled with the Butterworth-Van Dyke model illustrated in Fig. 1 [6-8]. This model contains a static capacitance C_p in parallel with an LCR branch modeling the PR's mechanical inertia, compliance, and loss properties, respectively. The PR's impedance characteristic is shown in Fig. 2, in which the resonant frequency (f_r) occurs at series resonance between L and C, and the anti-resonant frequency (f_{ar}) occurs at parallel resonance between C_p and the series LC branch. PTs are similarly modeled with the reduced Mason model shown in Fig. 3, which contains terminal capacitances, an LCR branch, and an ideal transformer [9-10].

Although piezoelectric components have been extensively utilized for sensing, actuation, transduction, and energy harvesting, their application in power electronics has been more limited. PTs have a long history that includes high-volume commercialization for CCFL backlight drivers [11], but demand for them waned with the advent of LEDs. Widespread adoption of piezoelectrics in other aspects of power electronics has been inhibited by the relatively poor efficiencies of available components and a limited understanding of how to utilize them without magnetic components. Today, new circuit designs and control techniques, improved semiconductor devices and integrated circuit technology, advanced piezoelectric materials and fabrication capabilities, and more sophisticated modeling and simulation tools constitute fertile technological ground for realizing the theoretical benefits of piezoelectrics in power electronics. However, manifesting the advantages of piezoelectrics will require fundamental reconsideration of both power electronic circuits and piezoelectric components themselves.

In this paper, we summarize recent progress, present challenges, and future opportunities for piezoelectric-based power conversion. Section II discusses power electronic circuit topologies, operating modes, and control, and Section III reviews piezoelectric component design, fabrication, and packaging. In Section IV, we examine the scalability of piezoelectrics through a set of case studies that reveal advantageous scaling characteristics for miniaturization.

Fig. 1. Butterworth-Van Dyke circuit model [6-8] and example PRs.

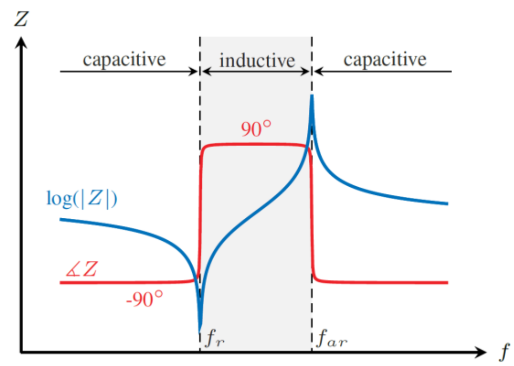

Fig. 2. PR impedance in the proximity of a vibration mode.

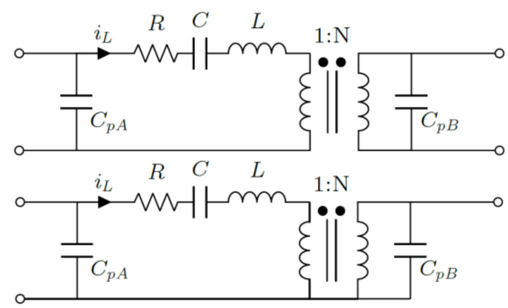

Fig. 3. Reduced Mason circuit model for isolated and non-isolated PTs [9-10].

II. Circuit Topologies, Operating Modes, and Control

Dc-dc converter designs based on piezoelectrics have historically relied on standard resonant converter implementations, which typically yield low efficiencies without auxiliary magnetics [12-27]. These designs effectively replace an LC or LCC resonant tank with a PR or PT, respectively. However, a piezoelectric component differs from a typical resonant tank in that it has non-negligible terminal capacitances and very high characteristic impedance $\sqrt{L/C}$. Efficient utilization of piezoelectric components requires power electronic circuit topologies, operating modes, and control strategies specifically tailored to the properties of piezoelectrics themselves.

A. Magnetic-less DC-DC Converter Implementations

In 2018 and 2019, [28-31] demonstrated that magnetic-less PR-based converters could achieve competitive efficiencies across wide operating ranges through use of specific six-stage switching sequences. A "six-stage switching sequence" cycles through six switch states, or "stages", every switching period. This includes three energy transfer stages in which both PR terminals are connected to the source-load system (i.e., "connected" stages), alternated with

978-1-6654-0756-4/22/$31.00 ©2022 IEEE

2022 IEEE Custom Integrated Circuits Conference (CICC) | 978-1-6654-0756-4/22/$31.00 ©2022 IEEE | DOI: 10.1109/CICC53496.2022.9772801

Table 1. Example six-stage switching sequences for step-down PR-based dc-dc converters [29,31,35]. Topologies correspond to Fig. 4.

Switching Sequence	Gain Range	Topology	Experimental Demonstrations
V_{in}-V_{out}, *Zero*, V_{out}	$V_{in} > V_{out}$	(a)	[31]: 114 kHz, V_{max} = 200 V, P_{max} = 25 W, η_{max} > 99%, PZT, radial mode [33]: 6.8 MHz, V_{max} = 60 V, P_{max} = 30.9 W, η_{max} = 96.5%, LN, thickness mode [34]: 6 MHz, V_{max} = 60 V, P_{max} = 32 W, η_{max} = 93.6%, LN, thickness mode
V_{in}, V_{in}-V_{out}, V_{out}	$V_{in} > V_{out} > ½V_{in}$	(a)	[31]: 114 kHz, V_{max} = 100 V, P_{max} = 8 W, η_{max} > 99%, PZT, radial mode [36]: 6.8 MHz, V_{max} = 60 V, P_{max} = 51 W, η_{max} = 96.7%, LN, thickness mode
V_{in}, *Zero*, V_{out}	$V_{in} > V_{out}$	(b)	[29]: 90 kHz, V_{max} = 30 V, P_{max} = 1.4 W, η_{max}=98.4%, PZT, radial mode (with step-up version of switching sequence and topology)
V_{in}-V_{out}, -V_{out}, *Zero*	$V_{in} > V_{out}$	(c)	N/A
V_{in}-V_{out}, -V_{out}, V_{out}	$½V_{in} > V_{out}$	(d)	[35]: 90 kHz, V_{max} = 120 V, P_{max} = 16 W, η_{max} > 95%, PZT, radial mode [35]: 1 MHz, V_{max} = 200 V, P_{max} = 100 W, η = 83.5%, PZT, thickness mode

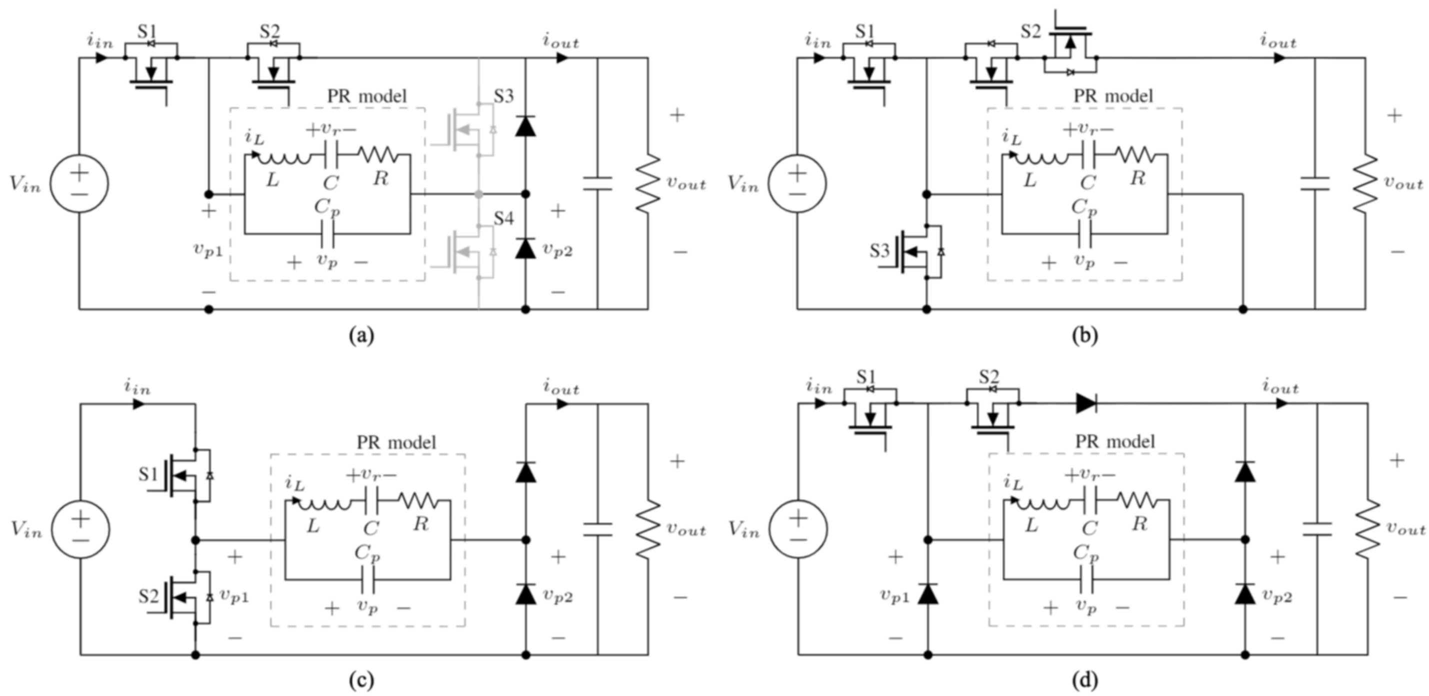

Fig. 4. Example circuit topologies for realizing the six-stage PR-based switching sequences shown in Table 1 [29,31,35].

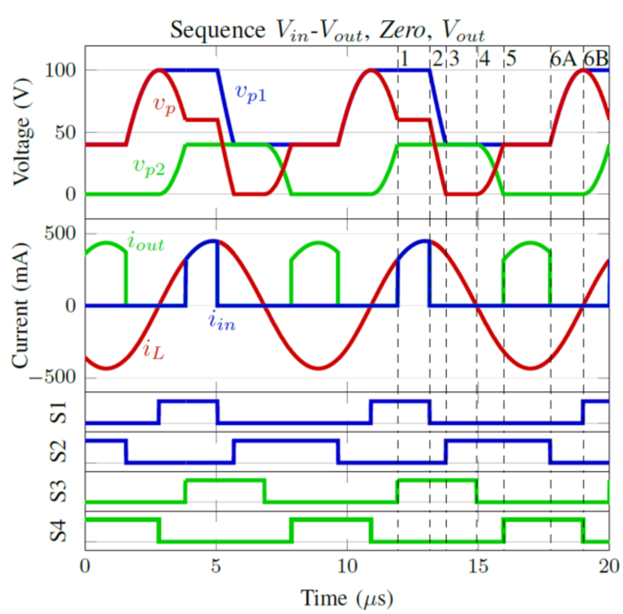

Fig. 5. Example waveforms for switching sequence V_{in}-V_{out}, *Zero*, V_{out} with V_{in}=100V and V_{out}=40V [31]. Stages denoted by number.

three resonant stages in which at least one terminal is open-circuited to allow resonance of C_p (i.e., "open" stages). We refer to switching sequences by listing the PR's connected-stage voltages (v_p) in chronological succession, assuming open stages between each. For example, sequence "V_{in}-V_{out}, *Zero*, V_{out}" corresponds to the topology of Fig. 4(a) and operates as shown in Fig. 5, cycling through stages with $v_p = V_{in}$-V_{out}, $v_p = 0$, and $v_p = V_{out}$ each switching period.

[29] has demonstrated a PR-based converter based on the six-stage switching sequence V_{in}, *Zero*, V_{out}, which can be realized with the topology shown in Fig 4(b) for step-down operation. In [31], potential PR-based converter switching sequences have been enumerated and down-selected to identify those capable of high-efficiency behaviors (e.g., zero voltage switching (ZVS) and minimal charge circulation) and practical characteristics (e.g., wide voltage gain ranges for regulation and simple switch implementations). This process revealed a set of practical dc-dc converter implementations capable of efficiently utilizing PRs across wide operating ranges as displayed in Table 1, including the highest-efficiency sequence V_{in}-V_{out}, *Zero*, V_{out} for mild step-down ratios. This switching sequence has been utilized for achieving high efficiency in multiple converter prototypes [31-34], the performances of which are also summarized in Table 1.

For a given V_{in}, V_{out}, and R_{load}, the periodic steady-state operation of a six-stage switching sequence is fully constrained by its high-efficiency behaviors. PR efficiency can be estimated using the amplitude of resonance model detailed in [31], which approximates the amplitude of the PR's assumed-sinusoidal i_L based on the total

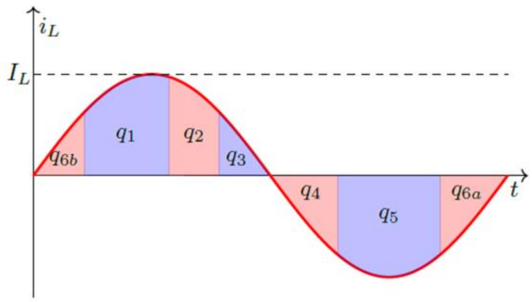

Fig. 6. Sinusoidal approximation of i_L and resulting amplitude of resonance I_L, based on the charge transfer of each stage, using V_{in}-V_{out}, *Zero*, V_{out} (displayed in Fig. 5) as an example [31].

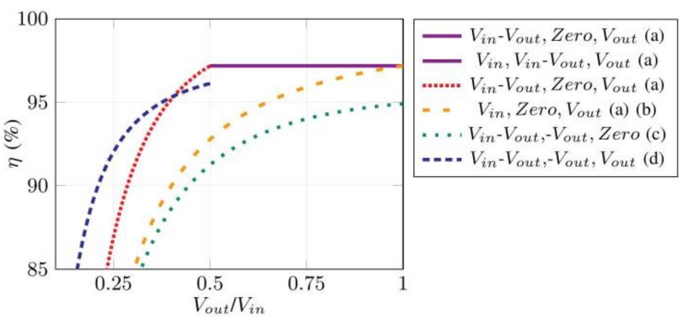

Fig. 7. Efficiency comparison between switching sequences using the example PR in [31] with V_{in} = 100 V and P_{out} = 10.0 W.

quantity of charge it displaces each resonant cycle as visualized in Fig. 6. We use this model to display the efficiency capabilities of certain switching sequences in Fig. 7 assuming the example PR parameters in [31]. All sequences provide continuous ranges of gain, and sequences V_{in}-V_{out}, *Zero*, V_{out} and V_{in}, V_{in}-V_{out}, V_{out} are capable of constant-efficiency voltage regulation for $V_{in} > V_{out} > ½ V_{in}$.

One limitation of these PR-based converter implementations is that efficiency decreases as voltage gain becomes more extreme. For the step-down case, this can be improved through switching sequences that spend a greater fraction of the PR's resonant period delivering energy to the load, which is explored in [35] with the V_{in}-V_{out}, -V_{out}, V_{out} sequence and the topology of Fig. 4(d). The efficiency capability of this switching sequence is also displayed in Fig. 7 and out-performs V_{in}-V_{out}, *Zero*, V_{out} for high step-down ratios. However, applications requiring even more extreme voltage gain will necessitate new converter architectures and operating approaches for efficient PR utilization.

An alternative solution for realizing extreme voltage gain is use of multi-port PTs, which offer inherent voltage transformation and the potential for galvanic isolation. In [37-39], isolated and non-isolated PT-based converter switching sequences capable of high efficiency across wide operating ranges have likewise been identified. These converter implementations each operate with a six-stage switching sub-sequence at one port and a simpler four-stage sub-sequence at the other, amounting to minimal added complexity over PR-based switching sequences. One such implementation is the V_{in}, *Zero+*, *Zero-* | V_{out}, V_{in} sequence (denoted "input port sub-sequence | output port sub-sequence") realized with the topology shown in Fig. 8, which operates with the waveforms shown in Fig. 9. In [38,39], a prototype of this implementation achieved an experimental whole-converter efficiency of 90% with an off-the-shelf PT. This is a significant improvement over previous magnetic-less dc-dc converter prototypes based on PTs, but it highlights a gap in achievable efficiency between designs based on presently-available PRs and PTs. There is hence an opportunity for new PT design techniques that harness the efficiency advantages of PRs as further discussed in Section III-B. There is also an opportunity to leverage PRs themselves for impedance compensation [40,41] and harmonic filtering [42] in PT-based converters.

Further opportunity lies in hybridization of switched-capacitor (SC) converters with piezoelectrics to provide both high voltage gain and efficient voltage regulation. SC converters can offer high-efficiency voltage transformation and discretely-changeable gains to complement the regulation capabilities of a piezoelectric-based converter (i.e., constant efficiency for the full $V_{in} > V_{out} > ½ V_{in}$ operating range as shown in Fig. 7). As with hybrid SC/magnetics designs [43-46], this approach may consist of separate cascaded stages or merged operation for soft-charging of the SC stage.

Although periodic steady-state operation of a six-stage sequence is fully constrained, additional degrees of freedom may be obtained through alternating regular six-stage resonant cycles with other types of resonant cycles, creating "mixed" switching sequences. In [36], regular cycles of V_{in}, V_{in}-V_{out}, V_{out} are alternated with *Zero* cycles, in which the PR's terminals are short-circuited, allowing regulation of power at a fixed frequency. This operating strategy is useful for avoiding a PR's spurious modes, a component-level hindrance further discussed in Section III-B. One could likewise consider even more sophisticated switching schemes (e.g., 8+ stage sequences [31]) to achieve high performance and manage spurious modes. It may be appreciated that we are only at the outset of understanding how to best utilize piezoelectric components for high performance.

B. Control of Magnetic-less DC-DC Converter Implementations

One challenge of the PR-based dc-dc converter implementations described in Section II-A is that they require precise switch timing to maintain their high-efficiency behaviors. Controlling such timing involves elements of frequency modulation, pulse width modulation, dead time control, and phase shift between half-bridges, requiring an intricate closed-loop control strategy to achieve high performance.

Six-stage switching sequences consist of three connected stages, requiring two of these connected stages to share the same half-cycle (of same i_L polarity) as exemplified by stages 1 and 3 in Fig. 6. Modulating the time ratio between these two connected stages, which are collectively bounded by the half cycle, requires a change in V_{in} or V_{out} to rebalance energy within the PR [31,47]. The transition point between these stages therefore serves as a control handle for voltage regulation with high-efficiency behaviors as demonstrated in [29,47,48]; we refer to the switch pair responsible for this transition

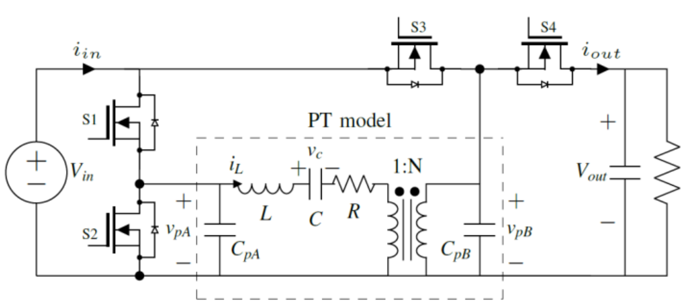

Fig. 8. Circuit topology for realizing the V_{in}, *Zero+*, *Zero-* | V_{out}, V_{in} PT-based switching sequence [38,39].

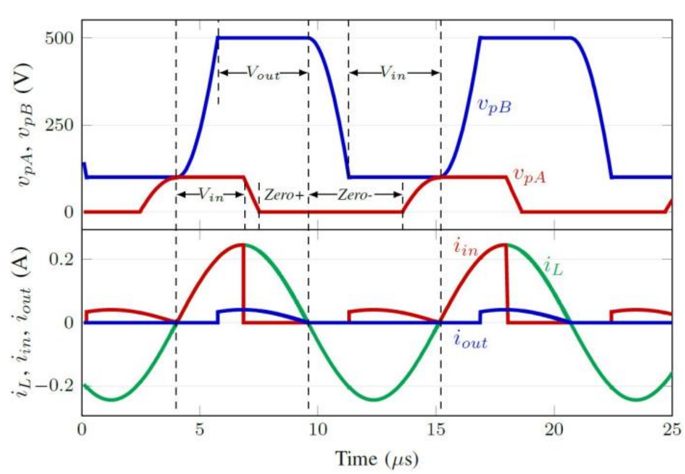

Fig. 9. Example waveforms for V_{in}, *Zero+*, *Zero-* | V_{out}, V_{in} with V_{in}=100V and V_{out}=500V [39]. Stages labeled by terminal voltage.

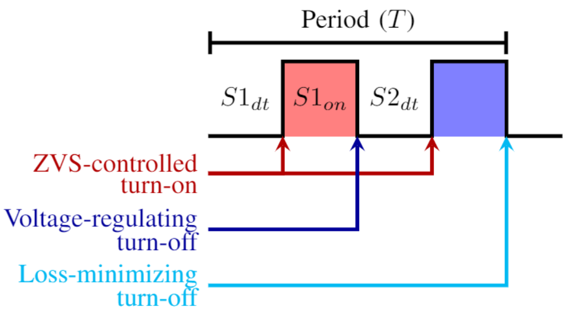

Fig. 10. Roles of the S1 and S2 switch transitions in Fig. 4(a) for the V_{in}-V_{out}, *Zero*, V_{out} switching sequence, and the resulting control variables for static closed-loop control [47].

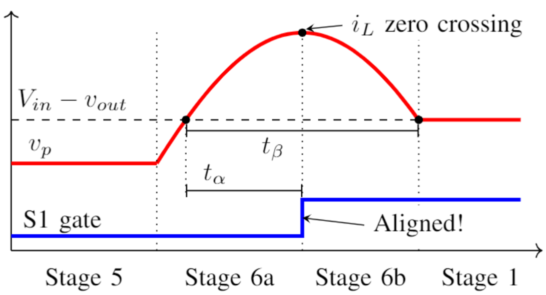

Fig. 11. Geometric detection of the i_L zero crossing for the V_{in}-V_{out}, *Zero*, V_{out} switching sequence. Due to assumed symmetry in the v_p waveform, the i_L zero crossing occurs at ½ t_β, or temporally halfway between two v_p crossings of the same voltage. In static control, T is controlled so that t_α, which corresponds to the turn-on of S1, aligns with ½ t_β [47].

as the "regulating switch pair". All other switching times are generally constrained for the high-efficiency behaviors of ZVS and minimum charge circulation. Frequency is also determined by these high-efficiency behaviors and varies throughout the PR's inductive region (illustrated in Fig. 2) for these six-stage sequences [31,33]. The frequency corresponding to a specific operating point can be estimated using the periodic steady-state solution [31], a charge-transfer-based approach, or a Fourier-based approach [49].

While the specific control implementations vary among [29,47,48,50] depending on switching sequence and topology, each can be implemented using only voltage sensing. For consistent operation, the switching sequence must be synchronized to the i_L waveform, which can be observed through detection of at least one i_L zero crossing. In [29,48] and "sensed control" in [47], the i_L zero crossing is detected by the voltage of a diode rising above zero after turning off, which occurs when i_L reverses polarity. This zero crossing triggers the start of a new switching period, so the only control variables are the switch on-time durations; frequency is determined passively rather than set by a controller. Although voltage-sensed switching has been used in high-frequency power converters (e.g., [51,52]), hardware limitations constrain the upper bound for switching frequency. Moreover, this approach is susceptible to high-frequency noise and interference due to spurious modes.

In [47], a "static" control strategy is demonstrated in which the switching period, duty cycles, and dead times are actively set by a controller rather than determined by triggering. For the V_{in}-V_{out}, *Zero*, V_{out} switching sequence, S1 and S2 constitute the regulating switch pair and can be statically controlled using the strategy described in Fig. 10. In this example, the period (T), the S1 on-time ($S1_{on}$), and both switch dead times ($S1_{dt}$ and $S2_{dt}$) are all controlled with PI compensators according to the references shown in Table 2, with V_{out}^* indicating the desired output voltage. The on-time of S2 is determined passively based on these four variables. The i_L zero crossing is determined geometrically during stage 6 (an open stage) as visualized in Fig. 11, which also permits straightforward synchronous rectification. This method is implemented in [47] using

Table 2. Control loop parameters for static control of the V_{in}-V_{out}, *Zero*, V_{out} sequence. Variables correspond to Figs. 10, 11 [47].

Control Variable	Sensed Input	Reference Value	Measurement Trigger
$S1_{on}$	v_{out}	V_{out}^*	N/A
$S1_{dt}$	v_{p1}	V_{in}	S1 turn-on
$S2_{dt}$	v_{p1}	v_{out}	S2 turn-on
T	t_α	½ t_β	N/A

a microcontroller. Additional i_L synchronization strategies are discussed in [50] in the context of PT-based converters.

There is tremendous opportunity for additional control strategies that are suitable for high frequencies and are robust to spurious modes, along with extensions of existing methods to PT-based implementations, mixed sequences, startup, and burst-mode operation [53]. To reduce system component count and power consumption in practical converter designs, there will also be a significant need for integrated controllers based on these strategies.

C. Other Applications in Power Electronics

Beyond magnetic-less dc-dc converters, piezoelectric components are attractive for a variety of other applications in power electronics. In [54,55], a PR is leveraged for second harmonic cancellation in a class Φ_2 resonant inverter, providing superior filtering with significantly lower loss than a comparable inductor and capacitor branch. A PR also replaces the discrete inductor and capacitor branch of a Class E inverter in [56], resulting in higher efficiency and power density. Further, piezoelectric components have been used to reduce the sizes of EMI filters through selective frequency filtering, which is demonstrated in [57]. Multi-port piezoelectric components yielding high efficiency and small physical volume can likewise be envisioned for functions usually associated with RF applications (e.g., filters, power combiners, transmission-line transformers, etc.). A myriad of other opportunities exists for piezoelectrics to enable higher performance and power density in power electronics.

III. Component Design, Fabrication, and Packaging

Equally important to piezoelectric-based power electronic circuit architectures are high-performance piezoelectric components themselves. While component design and realization strategies have been developed for other applications, power conversion presents a unique set of needs and challenges.

A. Piezoelectric Materials and Vibration Modes

Historically, the most common type of piezoelectric material is lead zirconate titanate (PZT), which has seen utilization in a wide variety of applications. Lithium niobate has also emerged as a promising material for power conversion primarily due to its high quality factor (Q_m > 10,000), which translates to high efficiency capability. Piezoelectric components can be manufactured in a wide variety of shapes, electrode patterns, and crystal orientations, and the combination of these (in addition to their boundary conditions) determines their potential vibration modes. These vibration modes can be broadly categorized as "parallel" modes or "perpendicular" modes, for which the applied and induced electric fields are parallel or perpendicular, respectively. Examples of promising vibration modes for power conversion are shown in Fig. 12.

Criteria for evaluating piezoelectric materials and vibration modes for power PRs have been derived in [33,58,59] in the context of a realistic converter switching sequence, including open stages. In [59], the minimum loss ratio (and therefore maximum efficiency) of a PR is found to be a function of only its mechanical quality factor Q_m and electromechanical coupling coefficient k. The inverse of this minimum loss ratio constitutes a figure of merit (FOM) for piezoelectric materials with the following reduced form for most vibration modes (if we approximate 8 ≈ π^2) [58,59]:

$$\mathrm{FOM}_m \propto Q_m \frac{k^2}{1-k^2}\left(1+\sqrt{1-k^2}\right) \qquad (1)$$

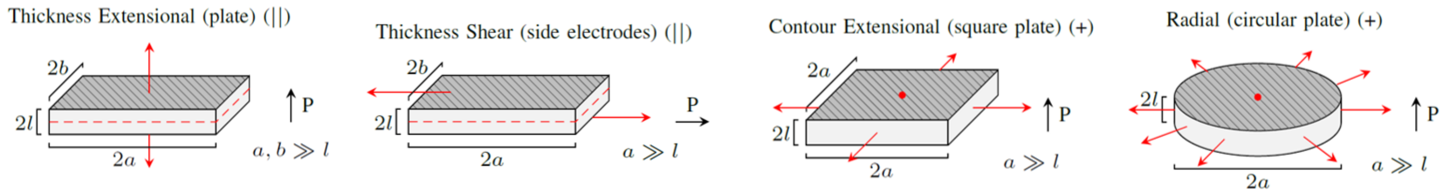

Fig. 12. Example parallel (II) and perpendicular (+) PR vibration modes for power conversion. Electrodes have area *A* and are denoted by shaded areas, displacement direction(s) are marked with red arrows, and nodes / nodal planes marked with red dots / dashed lines, respectively. The polarization direction of the PR is denoted with 'P', and all surfaces are assumed to be traction-free [8,54].

For the highest-efficiency V_{in}-V_{out}, *Zero*, V_{out} operating region, this minimum loss ratio occurs at an operating frequency of $\bar{f} = \frac{2f_r f_{ar}}{f_r + f_{ar}}$ (not at the series resonant frequency), and it corresponds to a specific geometry condition that informs PR design.

A simpler version of this figure of merit ($Q_m k^2$) is also proposed in [33], though it loses correspondence with the six-stage switching sequence minimum loss ratio for high values of *k*. Both figures of merit consider only mechanical loss, which is dominant near the resonant frequency [60], though the effect of dielectric loss is also explored in [33].

In [59], figures of merit are also derived for volumetric energy handling density (i.e., volumetric power density normalized to frequency), and areal power density (i.e., footprint density). These quantities each depend on only material properties and a geometry-normalized maximum I_L (I_{Lmaxo}), which can be constrained by material limits for stress and electric field as well as thermal management limits. Like the minimum loss ratio, these power density maxima correspond to specific geometry conditions to aid PR design. Maximum volumetric energy handling density (VED) and areal power density (APD) have the following forms, respectively:

$$\text{FOM}_{VED} = \frac{{I_{Lmaxo}}^2}{\varepsilon^T(1-k^2)\overline{K_o}^2 {v_a}^2} \quad (2)$$

$$\text{FOM}_{APD} = \frac{{I_{Lmaxo}}^2}{\pi \varepsilon^T(1-k^2)\overline{K_o} v_a} \quad (3)$$

Where ε^T is the constant-stress dielectric constant, v_a is the acoustic velocity, and $\overline{K_o}$ is the geometry-normalized wave number corresponding to $\bar{f}$ (e.g., $\overline{K_o} = \frac{2\pi \bar{f} l}{v_a}$ for parallel modes). Regarding these FOMs, we note that areal quantities for perpendicular modes may have operating point dependence as further detailed in [59].

This theoretical framework provides criteria for comparing piezoelectric materials and vibration modes, revealing the trends shown in Tables 3 and 4. The geometry condition corresponding to maximum efficiency requires perpendicular modes to be more planar, though these modes are capable of higher power density for a given frequency. Modes for which the electrode plane doesn't laterally expand may be advantageous for mounting, and modes that leverage the component's longest length dimension are less prone to spurious modes. In terms of materials, lithium niobate has significantly higher efficiency capability than PZT, though the characteristic impedance of lithium niobate requires more extreme planar form factors. Other materials such as aluminum nitride and gallium nitride are presently limited by a low *k*. Several material candidates are compared in [33,34,59].

This analysis has assumed piezoelectric material properties and Q_m to be constant with respect to frequency, amplitude of resonance, and temperature. For high power density, piezoelectric components will be pushed to extremes along all three of these axes, but how their collective properties will change is not yet well understood. Investigation and better quantification of material performance vs. frequency, excitation level, and temperature will be important for advancing the design of these components.

B. Piezoelectric Component Design

Once a piezoelectric material and vibration mode have been selected, a piezoelectric component's dimensions can be designed to achieve maximum efficiency and power density at a nominal converter operating point. The PR geometry conditions

Table 3. Comparison of vibration modes for power conversion

Mode Type:	Parallel	Perpendicular
Power density:	Higher APD	Higher VED
Required geometry:	Planar	Extremely planar

Table 4. Comparison of materials for power conversion

Material:	Hard PZT	Lithium Niobate
Efficiency	High	Extremely high
Required geometry:	Planar	Extremely planar

corresponding to minimum loss ratio and maximum power density discussed in Section III-A are orthogonal, so both may be satisfied in a single PR design. These geometry conditions have the forms [59]:

$$\hat{G} = \frac{4\pi}{\varepsilon^T(1-k^2)\overline{K_o} v_a} \frac{P_{out}}{{V_{in}}^2} \quad (4)$$

$$\hat{l} = \frac{\varepsilon^T(1-k^2)\overline{K_o} v_a}{2} \frac{V_{in}}{I_{Lmaxo}} \quad (5)$$

where $\hat{G} = A/l^2$ for parallel modes and $\hat{G} = A/(al)$ for perpendicular modes. These geometry conditions are analogous to selecting f_r and C_p for most vibration modes. A similarly-derived C_p condition for maximum efficiency is provided in [33].

One of the foremost challenges for piezoelectric component design is spurious modes, or minor resonant modes, in the proximity of a desired resonant mode. Spurious modes are typically harmonics of other vibration modes and cause a component's impedance to locally stray from the ideal characteristic shown in Fig. 2. This can severely limit the performance and operating region of a PR, particularly for converter use cases that span the inductive frequency region and depend on inductive phase for ZVS like the six-stage dc-dc converter switching sequences discussed in Section II-A. Spurious modes have negatively affected the performance of several prototypes discussed herein (e.g., [29,31,33]).

Strategies for minimizing the impact of spurious modes have been explored in [33,34,36,61]. Vibration modes that are set by length dimensions other than the longest (i.e., thickness and shear modes) tend to be more vulnerable to spurious modes, but use of circular shapes for these PRs rather than rectangular shapes can reduce them as shown in [34]. An alternative strategy involves designing piezoelectric components with dimensions that place spurious modes outside the frequency range of interest as demonstrated in [33]. For six-stage sequences that span a component's inductive region, circuit-level control strategies may also be leveraged to avoid spurious mode frequencies as shown in [36] and discussed Section II-A. There is a need for additional component-level design solutions that minimize the effects of spurious modes on performance.

Significant opportunity lies in piezoelectric component "augmentation", defined to be the attachment of mass and/or a spring-like material to the dynamic surfaces of a piezoelectric material, creating a composite electromechanical energy storage component. Fig. 13 illustrates an example of this concept in which a thickness mode PR is augmented with thin layers of mass on its two

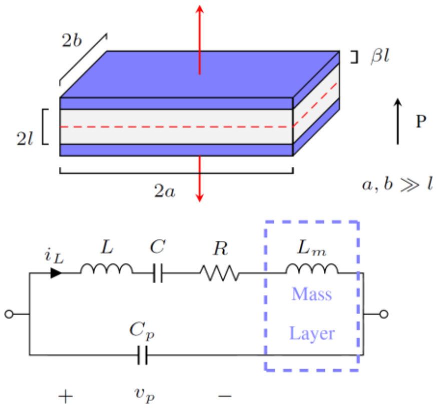

Fig. 13. Thickness vibration mode of a mass-augmented PR. The added mass layers manifest as an additional inductance in the PR's impedance and circuit model [62].

electrode surfaces. As shown analytically in [62], such mass augmentation results in monotonic increases in efficiency and power density with respect to the mass's relative size, assuming the PR's *R* is unchanged. Similar advantages may exist for a variety of vibration modes and component structures. Thus, composite energy storage elements that leverage the transduction of a piezoelectric material and the inertial and/or compliant energy storage of other material(s) open possibilities for even higher performance.

While most commercially-available PRs were developed for other applications, PT development has been rooted in power conversion [10,11,63-73]. Despite such progress, commercially-available PTs are not competitive with PRs in terms of efficiency without auxiliary magnetic components. While this may be partly attributed to imperfect mechanical coupling between a PT's primary and secondary halves, there is an opportunity to leverage what is now understood about designing PRs to design PTs with dramatically greater performance capabilities. This will require an intersection of low-loss piezoelectric materials, high-efficiency vibration modes, and intentional geometry selection for maximum efficiency and power density. High-performance PTs will enable a variety of power conversion applications requiring extreme gain and/or isolation.

C. Fabrication and Packaging

Fabrication procedures for discrete piezoelectric components vary with material and are discussed in [74,75]. Because piezoelectric materials are anisotropic, the crystal orientation within the piezoelectric component dictates its effective material properties and compatible vibration modes [75]. PZT-based converter prototypes in [29,31,35] have been based on commercially-available components, but quasi-thickness mode lithium niobate PRs have been fabricated in [33,34]. Both of these fabricated components are based on a +36° Y-cut crystal orientation, which provides the highest k_t for lithium niobate [75]. The performance of these PRs is displayed in Table 1. An opportunity for higher coupling coefficients for lithium niobate PRs lies in shear modes, which can be realized through X-cuts [34,59].

Very high theoretical quality factors (i.e., for materials such as lithium niobate) are challenging to physically realize in piezoelectric components. This is due to mechanical damping caused by mounting as well as resistance in the electrodes and electrical attachments. Solder connections introduce prohibitive mechanical loss for small-scale bulk PRs, but opportunity lies in spring-based mounting structures capable of maintaining reliable electrical connection. As demonstrated in [33,34], PRs can also be fabricated with "inactive" areas of material that extend wider than their electrodes; these inactive areas can then be used to fix the component to a surface. Aluminum wire bonding has been explored in [33,36] for realizing low-loss electrical contacts, with a higher quantity of such wires being advantageous for efficiency. There is further opportunity to minimize acoustic coupling and loss through Bragg reflectors, which have been explored in MEMS resonators for non-power applications [76]. In summary, there is great demand for PR mounting and packaging solutions that introduce minimal added volume, minimal mechanical damping, maximum thermal conductivity, and protection against mechanical disturbances.

D. Integration

Integrated power electronic systems promise smaller-size, higher-performance, and lower-cost power delivery [77]. Unlike magnetics, piezoelectrics are conducive to higher degrees of integration in terms of both process compatibility and scalability, which is further discussed in Section IV. There is thus opportunity to leverage piezoelectrics in designing fully-integrated discrete power modules as well as heterogeneously-integrated systems in package including power management. Piezoelectric materials do have precedent in integrated systems; lithium niobate and aluminum nitride have been widely used in surface acoustic wave and bulk acoustic wave filters for RF applications [75,78]. Important challenges to address for integrating power piezoelectric components include fabrication process compatibility, mounting, thermal management, and software tools for co-designing piezoelectric, analog, and digital components.

Looking in another direction, electrostatically-driven resonators can be fabricated in silicon through MEMS processes and offer similar equivalent circuit models to that of Fig. 1 [79]. The circuit, control and other ideas described herein may thus be leveraged to realize high-performance power conversion based on lumped micro-mechanical structures. Moreover, transformer-like micromechanical structures have also been envisioned for power conversion [80-82]. Outside of [79-82], these concepts have received almost no attention in the power conversion context but may offer a fruitful direction for future research, especially for integrated low-power systems.

IV. Scalability

The most compelling opportunity presented by piezoelectrics to power conversion is favorable scalability to small sizes. We now examine the scaling properties of piezoelectrics through the lens of a PR. To do so, we assume that a PR design follows the geometry conditions in (4) and (5) for maximum efficiency and power density, respectively. We also assume a fixed I_{Lmaxo} based on a fixed electric field, stress, or loss density limit as described in [59]. The geometry conditions then constrain all dimensions of the component, and therefore its resonant frequency, based on a nominal operating point (i.e., P_{out} and V_{in}, assuming the V_{in}-V_{out}, *Zero*, V_{out} sequence). For perpendicular modes, we note that I_{Lmaxo} is not independent of operating point for the loss-density-limited case, so this analysis only applies for stress or electric field limits [59].

With these constraints, a component design always achieves both the minimum loss ratio of (1) and the maximum densities of (2) and (3). The minimum loss ratio has no dependence on geometry, which implies that the achievable efficiency of a piezoelectric component is irrespective of size (to the extent that Q_m and k also remain the same). Further, the maximum volumetric energy handling density also has no dependence on geometry, which suggests that maximum volumetric power density rises linearly with frequency. Thus, achievable volumetric power density (at I_{Lmaxo}) rises linearly as the component's frequency-setting dimension scales down in size.

The effects of this scaling can be illuminated through case studies in which certain PR dimensions are scaled by factor α. We begin by scaling all three dimensions of a PR by α, which corresponds to a volume change of α^3. The resulting frequency, and therefore the achievable volumetric power density given I_{Lmaxo}, scales by α^{-1}, so both quantities rise as a component is scaled down in size (α<1). To satisfy the maximum power density geometry condition in (5), V_{in} must also scale by α, which then requires P_{out} to scale by α^2 to satisfy the maximum efficiency geometry condition in (4). This suggests that the greatest power density potential for piezoelectric components occurs as $\alpha \rightarrow 0$, which corresponds to low voltage, very low power, and high frequency components. These scaling characteristics are displayed in Fig. 14 and Table 5.

Realistically, manufacturing or application constraints may allow only partial scaling of a PR, so we next examine the independent scalability of PR dimensions *l* and *a*. The result is different between parallel and perpendicular vibration modes in part due to different frequency-setting dimensions but also due to different geometry conditions for maximum efficiency. Independently scaling *l* and *a* by

Table 5. PR scaling case studies constrained for fixed I_{Lmaxo}, maximum efficiency, and maximum power density

Case Study	Mode	Volume	Area	Thickness	f	V_{in}	P_{out}	Efficiency
Scale all dimensions by α	Any	α^3	α^2	α	α^{-1}	α	α^2	1
Scale l by α	Parallel	α	1	α	α^{-1}	α	1	1
	Perpendicular	α	1	α	1	α	α	1
Scale a by α	Parallel ($a \neq b$)	α	α	1	1	1	α	1
	Parallel (a=b)	α^2	α^2	1	1	1	α^2	1
	Perpendicular	α^2	α^2	1	α^{-1}	1	α	1
Scale a by α, and l by α^{-1}	Perpendicular	α	α^2	α^{-1}	α^{-1}	α^{-1}	1	1

α results in the effects summarized in Table 5; this includes scaling of the PR's form factor and frequency along with the required scaling of P_{out} and V_{in} to uphold the geometry conditions for maximum efficiency and power density.

Several conclusions can be drawn from Table 5. For parallel modes, V_{in} and P_{out} can be manipulated independently through l and a, respectively. However, decreasing l for lower V_{in} also corresponds to an increase in frequency and achievable power density given I_{Lmaxo}. The highest density therefore occurs as $V_{in} \to 0$; varying a for P_{out} has no effect on frequency or density. For perpendicular modes, P_{out} can be manipulated independently from V_{in} through a, though decreasing a results in higher frequency and power density. V_{in} can only be manipulated independently of P_{out} if a and l are scaled inversely, which directly manipulates the component's form factor. However, decreasing l (for lower V_{in}) and increasing a results in decreases for frequency and power density. Thus, for the same P_{out}, highest achievable density is achieved at higher V_{in} for perpendicular modes.

The general conclusion to be drawn from Table 5 and Fig. 14 is that piezoelectric components have highly favorable scaling characteristics for miniaturization, especially compared to their magnetic counterparts. Although promising, this analysis stems from a simple theoretical framework that does not consider potential high-frequency losses or nonlinear piezoelectric material properties, and miniaturization will require a thorough understanding of these factors as discussed in Section III-A.

V. Conclusions

The present technological landscape creates fresh opportunity for pursuing piezoelectrics as passive components in power electronics. Recent progress in six-stage switching sequences for piezoelectric-based dc-dc converters has demonstrated piezoelectrics to be capable of competitive efficiencies without the presence of magnetics. Circuit-level challenges to be addressed include realizing high voltage gain, with or without PTs, along with control complexity. Simple, robust control strategies, and their implementation as integrated controllers, are needed for practical designs.

Further, recent progress in piezoelectric component design and fabrication has established piezoelectric material, vibration mode, and geometry criteria for power conversion along with mounting strategies. Major challenges to address include spurious modes, damping due to mounting, and nonlinearity of material properties. Significant opportunity lies in piezoelectric component augmentation, new piezoelectric transformer design strategies, and integration.

The broad opportunity offered by piezoelectrics to power conversion is favorable scalability to small sizes. Through case studies constrained for fixed I_{Lmaxo}, maximum efficiency, and maximum power density, we have shown that the achievable power densities of piezoelectric components are greatest at the smallest scales. This scalability is highly advantageous for miniaturization, though further characterization of piezoelectric component behavior at high power density is warranted.

In the future, favorable scalability to small sizes and high degrees of integration could permit a reality in which several small power conversion "cells" out-perform large single-unit converters of equivalent total size. This may in turn open the door to extreme modularity as a strategy for achieving higher performance, greater reliability, lower cost, and expanded capability in power electronic systems. With further development, piezoelectric-based power conversion is positioned to open new possibilities for applications in computing, wireless communication, robotics, biomedical devices, renewable energy, and more.

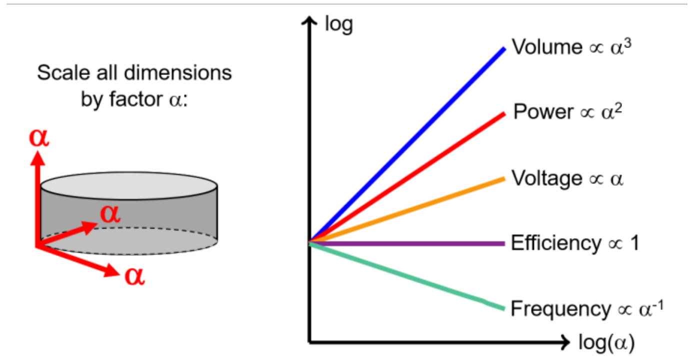

Fig. 14. PR scaling characteristics constrained for fixed I_{Lmaxo}, maximum efficiency, and maximum power density.

References:

[1] C. R. Sullivan *et al.*, "On size and magnetics: Why small efficient power inductors are rare," 3D-PEIM, Jun. 2016.

[2] D. J. Perreault *et al.*, "Opportunities and challenges in very high frequency power conversion," APEC, Feb. 2009.

[3] A. J. Hanson *et al.*, "Measurements and performance factor comparisons of magnetic materials at high frequency," TPEL, 2016.

[4] P. A. Kyaw *et al.*, "Fundamental examination of multiple potential passive component technologies for future power electronics," TPEL, 2018.

[5] A. M. Flynn and S. R. Sanders, "Fundamental limits on energy transfer and circuit considerations for piezoelectric transformers," TPEL, 2002.

[6] K. S. Van Dyke, "The piezo-electric resonator and its equivalent network," Proceedings of the Institute of Radio Engineers, 1928.

[7] S. Sherrit *et al.*, "Comparison of the Mason and KLM equivalent circuits for piezoelectric resonators in the thickness mode," IUS, Oct. 1999.

[8] J. Erhart *et al.*, *Piezoelectric Ceramic Resonators*. Springer, 2017.

[9] W. P. Mason, *Electromechanical Transducers and Wave Filters*. D. Van Nostrand Co., 1948.

[10] C. Lin, "Design and analysis of piezoelectric transformer converters," Ph.D. dissertation, Virginia Tech, 1997.

[11] A. Vazquez Carazo, "Piezoelectric transformers: An historical review," Actuators, MDPI, 2016.

[12] G. S. Seo *et al.*, "A magnetic component-less series resonant converter using a piezoelectric transducer for low profile application," ECCE Asia, Jun. 2010.

[13] S. Moon and J. H. Park, "High power dc–dc conversion applications of disk-type radial mode Pb (Zr, Ti) O_3 ceramic transducer," JJAP, 2011.

[14] A. M. Imtiaz *et al.*, "Contour-mode ring-shaped AlN microresonator on Si and feasibility of its application in series resonant converter," TPEL, 2014.

[15] R. L. Lin *et al.*, "Inductor-less piezoelectric transformer electronic ballast for linear fluorescent lamp," APEC, Mar. 2001.

[16] S. Bronstein and S. Ben-Yaakov, "Design considerations for achieving ZVS in a half bridge inverter that drives a piezoelectric transformer with no series inductor," PESC, Jun. 2002.

[17] M. Sanz *et al.*, “Magneticless converter based on piezoelectric transformers for step-down dc/dc and low power application,” APEC, Feb. 2003.

[18] S.-Y. Chen and C.-L. Chen, “ZVS considerations for a phase-lock control dc/dc converter with piezoelectric transformer,” IECON, Nov. 2006.

[19] J. M. Alonso *et al.*, “A novel control method for piezoelectric-transformer based power supplies assuring zero-voltage-switching operation,” TIE, 2008.

[20] M. Rodgaard *et al.*, “Empiric analysis of zero voltage switching in piezoelectric transformer based resonant converters,” PEMD, Mar. 2012.

[21] M. S. Rødgaard *et al.*, “Forward conduction mode controlled piezoelectric transformer-based PFC LED drive,” TPEL, 2012.

[22] M. S. Rødgaard, “Bi-directional piezoelectric transformer based converter for high-voltage capacitive applications,” APEC, Mar. 2015.

[23] E. L. Horsley *et al.*, “Analysis of inductorless zero-voltage-switching piezoelectric transformer-based converters,” TPEL, 2012.

[24] M. P. Foster *et al.*, “Critical design criterion for achieving zero voltage switching in inductorless halfbridge-driven piezoelectric-transformer-based power supplies,” TPEL, 2015.

[25] M. Ekhtiari *et al.*, “State-of-the-art piezoelectric transformer-based switch mode power supplies,” IECON, Oct. 2014.

[26] M. Ekhtiari *et al.*, “Analysis of bidirectional piezoelectric-based converters for zero-voltage switching operation,” TPEL, 2017.

[27] M. Ekhtiari *et al.*, “Dynamic optimum dead time in piezoelectric transformer-based switch-mode power supplies,” TPEL, 2017.

[28] B. Pollet *et al.*, “A new inductorless DC-DC piezoelectric flyback converter,” ICIT, Feb. 2018.

[29] B. Pollet *et al.*, “A new non-isolated low power inductorless piezoelectric dc-dc converter,” TPEL, 2019.

[30] J. D. Boles *et al.*, “Enumeration and analysis of dc-dc converter implementations based on piezoelectric resonators,” COMPEL, Jun. 2019.

[31] J. D. Boles *et al.*, “Enumeration and analysis of dc-dc converter implementations based on piezoelectric resonators,” TPEL, 2021.

[32] W. Braun *et al.*, “Inductorless soft switching dc-dc converter with an optimized piezoelectric resonator,” APEC, Mar. 2020.

[33] W. Braun *et al.*, “Optimized resonators for piezoelectric power conversion,” OJPE, 2021.

[34] M. Touhami *et al.*, “Piezoelectric materials for the dc-dc converters based on piezoelectric resonators,” COMPEL, Nov. 2021.

[35] M. Touhami *et al.*, “A new topology of dc-dc converter based on piezoelectric resonator,” COMPEL, Nov. 2020.

[36] E. Stolt *et al.*, “Fixed-frequency control of piezoelectric resonator dc-dc converters for spurious mode avoidance,” OJPE, 2021.

[37] J. D. Boles *et al.*, “High-efficiency operating modes for isolated piezoelectric-transformer-based dc-dc converters,” COMPEL, Nov. 2020.

[38] E. Ng *et al.*, “Non-isolated dc-dc converter implementations based on piezoelectric transformers,” ECCE, Oct. 2021.

[39] J. D. Boles *et al.*, “Dc-dc converter implementations based on piezoelectric transformers,” JESTPE, 2022.

[40] B. Ju *et al.*, "Piezoelectric ceramic acting as inductor for capacitive compensation in piezoelectric transformer." IET Power Electronics, 2015.

[41] B. Ju *et al.*, "General rules for the inductive characteristics of a piezoelectric structure and its integration with piezoelectric transformer for capacitive compensation." SMS, 2021.

[42] B. Ju *et al.*, "Piezoelectric filter module used in harmonics elimination for high-efficiency piezoelectric transformer driving." TPEL, 2015.

[43] R. C. N. Pilawa-Podgurski and David J. Perreault. "Merged two-stage power converter with soft charging switched-capacitor stage in 180 nm CMOS," JSSC, 2012.

[44] D. M. Giuliano *et al.,* “Miniaturized low-voltage power converters with fast dynamic response,” JESTPE, 2014.

[45] Y. Li *et al.*, “Resonant switched capacitor stacked topology enabling high dc-dc voltage conversion ratios and efficient wide range regulation,” ECCE, Sept. 2016.

[46] C. Schaef and J. T. Stauth, “A highly integrated series–parallel switched capacitor converter with 12 V input and quasi-resonant voltage-mode regulation,” JESTPE, 2018.

[47] J. J. Piel *et al.*, “Feedback control for a piezoelectric-resonator-based dc-dc power converter,” COMPEL, Nov. 2021.

[48] M. Touhami *et al.*, “Implementation of control strategy for step-down dc-dc converter based on piezoelectric resonator,” ECCE Europe, Sep. 2020.

[49] L. de Araujo Pereira *et al.*, “Operating frequency prediction of piezoelectric dc-dc converters,” TPEL, 2021.

[50] Z. Yang *et al.*, “Resonant current estimation and phase-locked loop feedback design for piezoelectric transformer-based power supplies,” TPEL, 2020.

[51] S. Lim *et al.*, “Two-stage power conversion architecture suitable for wide range input voltage,” TPEL, 2015.

[52] A. J. Hanson *et al.*, “A high-frequency power factor correction stage with low output voltage,” JESTPE, 2020.

[53] D. Vasic *et al.*, “Piezoelectric transformer-based dc/dc converter with improved burst-mode control,” ECCE, 2013.

[54] M. Vincent *et al.*, "A new topology of resonant inverter including a piezoelectric component." ECCE Europe, Sept. 2021.

[55] E. Stolt *et al.*, “Piezoelectric resonator second harmonic cancellation in class Φ_2 inverters,” COMPEL, Nov. 2021.

[56] C. Daniel *et al.*, “Class E power amplifier with piezoelectric resonator output branch,” COMPEL, Nov. 2021.

[57] F. Hubert *et al.*, “Piezoelectric EMI filter for switched-mode power supplies." TPEL, 2021.

[58] J. D. Boles *et al.*, “Evaluating piezoelectric materials for power conversion,” COMPEL, Nov. 2020.

[59] J. D. Boles *et al.*, “Evaluating piezoelectric materials and vibration modes for power conversion,” TPEL, 2022.

[60] K. Uchino and S. Hirose, “Loss mechanisms in piezoelectrics: how to measure different losses separately,” TUFFC, 2001.

[61] J. Forrester *et al.*, “Influence of spurious modes on the efficiency of piezoelectric transformers: A sensitivity analysis,” TPEL, 2020.

[62] J. E. Bonavia *et al.*, “Augmented piezoelectric resonators for power conversion,” COMPEL, Nov. 2021.

[63] G. Ivensky *et al.*, “Generic operational characteristics of piezoelectric transformers,” TPEL, 2002.

[64] E. Horsley *et al.*, “State-of-the-art piezoelectric transformer technology,” ECCE Europe, Sept. 2007.

[65] K. S. Meyer *et al.*, “Parameterized analysis of zero voltage switching in resonant converters for optimal electrode layout of piezoelectric transformers,” PESC, Jun. 2008.

[66] A. M. S´anchez *et al.*, “Design of piezoelectric transformers for power converters by means of analytical and numerical methods,” TIE, 2008.

[67] Y.-P. Liu *et al.*, “Design of fixed frequency controlled radial-mode stacked disk-type piezoelectric transformers for dc/dc converter applications,” SMS, 2009.

[68] S. Dong *et al.*, “Equivalent circuit and optimum design of a multilayer laminated piezoelectric transformer,” TUFFC, 2011.

[69] M. Khanna *et al.*, “New tunable piezoelectric transformers and their application in dc dc converters,” TPEL, 2017.

[70] X. Li *et al.* "Tunable High-Power Multilayer Piezoelectric Transformer." TIE, 2020.

[71] L. Wang *et al.*, “Comprehensive analysis of models and operational characteristics of piezoelectric transformers,” APEC, Mar. 2020.

[72] J. Forrester *et al.*, “RadPTDesigner: A program for designing radial mode piezoelectric transformers for inductorless inverters." ECCE Europe, Sept. 2021.

[73] B. Ju *et al.*, "Single-layer Piezoelectric Transformers with a Unique Design of Polarization Topologies." Sensors and Actuators A: Physical, 2021.

[74] R. Ghodssi and P. Lin, *MEMS Materials and Processes Handbook*, Springer, 2011.

[75] H. Bhugra and G. Piazza, “Piezoelectric MEMS Resonators”. Springer, 2017.

[76] W. Wang and D. Weinstein, "Acoustic Bragg reflectors for Q-enhancement of unreleased MEMS resonators," EFTF-IFCS, May 2011.

[77] “Chapter 10: Integrated Power Electronics,” *Heterogeneous Integration Roadmap*, IEEE Electronics Packaging Society, Nov. 2021.

[78] S. Gong *et al.*, "Microwave Acoustic Devices: Recent Advances and Outlook." JMW, 2021.

[79] J. Phinney, “Multi-Resonant Passive Components for Power Conversion,” Ph.D. thesis, MIT, June 2005.

[80] J. M. Noworolski and S. R. Sanders, “An electrostatic microresonant power conversion device”, PESC, Jun. 1992.

[81] J. M. Noworolski and S. R. Sanders, “Microresonant devices for power conversion”, SPIE Micromachine Devices and Components, Sep. 1998.

[82] J.M. Noworolski, “Micromechanical Power Conversion,” Ph.D. thesis, UC Berkeley,1998.